ORIGINAL ARTICLE

Research on deep drawing process with electro-permanent magnetic blank holder for non-ferromagnetic materials

Sicheng He[1,2] · Yonggen Sun[1,2] · Hongsheng Zhang[1,2] · Teng Zhang[1,2] · Shangbin Zhang[1,2] · Jiacheng Zhang[1,2] · Siji Qin[1,2]

Abstract
Through comparing the distribution of blank holder force (BHF) and stress-strain curve along the radial direction, there has been good forming capability and adaptability in deep drawing with the electro-permanent magnetic (EPM) blank holder (EPMBH) technique. However, whether the BHF technique is applicable for non-ferromagnetic materials has yet to be researched. In the paper, taking 08-Al steel and H62 copper plates as examples, the drawability of ferromagnetic and non-ferromagnetic sheets with EPMBH is investigated. Moreover, a series of confirmatory tests were carried out based on numerical analysis. It found that similar to the deep drawing with ferromagnetic slab, there is slight attenuation on the holding effect for non-ferromagnetic sheets, and the effect of gap on the magnetic attraction caused by the magnetic properties of the plate first increases sharply and then slowly decreases, while its possible failure modes are also wrinkling and rupture due to insufficient BHF and excessive drawing height, respectively. In the experiment, flawless deep-drawing workpieces can be obtained with EPMBH, indicating that EPMBH could meet the forming requirement for ferromagnet and non-ferromagnetic plates and can be controllably adjusted through altering the excitation current of the EPMBH device. The experiment result shows that the optimal excitation current is 14 A for ferromagnetic steel plate and 13 A for non-ferromagnetic copper plate with the same diameter of 110 mm and thickness of 0.8 mm.

1 Introduction

There is a high material utilization rate, streamlined microstructure, and good stiffness-to-weight ratio for the workpiece formed through a deep drawing process, which makes it indispensable in vehicle, transportation, and aerospace applications. In deep drawing, the BHF plays a crucial role in forming feasibility and its contour. In addition to suppressing wrinkling in the thickness direction of the sheet metal [1], BHF can also generate friction force [2] between the metal plate and the mold to control metal flow, thereby reducing rebound, improving forming quality, and forming limit. However, if BHF is insufficient, it is unable to complete the blank holder function or suppress sheet warping, and the problem of wrinkling may occur, while, if BHF is excessive, the metal hardly flows plastically except for the local region, increasing the risk of rupture.

In order to avoid wrinkling, Lee [3] investigated the impact of BHF on the fabric preforms in stamping forming operations. To better illustrate the phenomenon that under transverse load restraint, structural buckling is different from common bifurcation problems, the energy method is utilized to explore the stability of post-buckling and prove the existence of an energy barrier depending on the restraint and perturbation energy, which could suppress flange wrinkling under constant BHF. Through enhancing the binder force, Ayachi [4] formed a U-shaped thin plate with uniformly distributed residual stress in the thickness direction and declared that the internal stress generated by

✉ Siji Qin
plastics@ysu.edu.cn

1   School of Mechanical Engineering, Yanshan University, Qinhuangdao 066000, China

2   Advanced Forging Technology and Science Key Laboratory of Ministry of Education, Yanshan University, Qinhuangdao 066000, China

higher BHF is conducive to attenuating the local moment effect in bending. Through simulation, Sheng [5] adjusted the magnitude of BHF continuously with an adaptive simulation strategy to improve the drawing performance of non-symmetric parts. Kitayama [6] optimized the blank shape as well as the VBHF trajectory simultaneously with the sequential approximate method. Combining a neural network with a genetic algorithm, Wang [7] analyzed the impact of BHF on the dimension precision and surface quality of deep-drawing workpieces and pointed out that the wrinkling problem could be avoided with a two-stage hydraulic loading path. Tran [8] accurately predicted varying BHF for minimum earing height variation and a new magneto-rheological actuator was developed to mitigate the contradiction between forming efficiency and process stability.

Common BHF is loaded with a rigid or variable blank holder, where spring [9], rubber [10], and gas cushion are adopted as executive components. As a concise operating method, rigid loading can provide constant displacement with hydraulic equipment [11]. However, the rigid blank holder would suppress the plastic flow of the workpiece and reduce the uniformity of radial thickness. In fact, during the deep drawing process, the optimal BHF for the sheet slab would vary with time and position. Therefore, to improve forming limit and flow uniformity, the research on BHF mainly focuses on controllable and variable amplitude BHF. Air cushion can provide a constant BHF. In addition, BHF proportional to displacement can be obtained with spring blank, while rubber will cause that BHF increases sharply with displacement.

Nevertheless, the above-mentioned blank holder methods can only provide variable BHF loadings along specific paths, not achieving the goal of arbitrary adjustment of the BHF by the flexible edge holder. Furthermore, utilized to load BHF, the existing device not only requires a blank holder as an actuator but also requires a transmission and power system. The transmission system is generally mechanical transmission, where there is an obvious problem of operational wear and energy loss. Through spring or rubber, the common power source of BHF can be shared with that during the forming process. Detailly, the slider of the press machine descends and the blank holder first comes into contact with the concave mold to load the BHF in a non-fixed connection manner. The spring and rubber ensure the blank holder remains stationary, while the slide can continue to move downwards. Then, the punch installed on the slide of the press acts on the metal sheet for stamping. On the other hand, within the rigid blank holder, the function is completed by auxiliary hydraulic devices, namely, a double-action hydraulic press [12, 13].

In view of the above problem, EPMBH technology is proposed to ensure controllable BHF, which only needs to be energized twice for magnetization and demagnetization. Compared with an electromagnetic blank holder [14, 15], much less energy would be consumed and the power resource is integrated with the transmission system together in the electromagnetic cushion for lightweight. Based on EPM technology, Qin [16, 17] introduced a novel blank holder method that can independently load BHF during sheet metal forming and verified the feasibility of EPMBH. Zhang [18] investigated the thermal field and coupled magnetic-mechanical fields of EPMBH, and the result shows that the maximum temperature of the EPM cushion was about 54 °C after working for 3 h, which did not affect the normal use. With the radial segmental blank holder based on EPM, a more reasonable distribution of BHF can be realized, and the forming limit can be further improved by inhibiting wrinkling in the experiment [19]. The novel BHF method greatly simplifies the drawing equipment and satisfies the lightweight requirements of the equipment.

Due to the fact that the EPMBH force is from the permanent magnetic attraction, the magnetic properties of the workpiece play a significant impact on the stamping performance. Therefore, with ferromagnetic 08-Al steel plate and non-ferromagnetic H62 copper sheet, the deep drawing process was simulated and experimented. In the end, the drawing performance is compared through strain distribution and forming contour.

2 Principle

In the proposed deep drawing process with an EPM cushion, the contour of the blank holder is similar to that of a traditional blank holder. However, additional drive or transmission equipment is unnecessary, and the force cycle is limited between the blank holder and the suction plate, as shown in Fig. 1a. In detail, the BHF is generated by electromagnetic interaction without medium, which conducts and offsets through the metal slab. Figure 1b illustrates the model of an EPM device, which is mainly composed of multiple electromagnetic pole units (EPU). Besides, EPU consists of four permanent magnets (PM, Nd-Fe-B); a reversible magnet (RM, Al-Ni-Co); a conductive magnet (CM, Iron); and a copper coil. As seen in Fig. 1c, the side wall of CM keeps in contact with PM, whose bottom surface is located on RM, and RM is wrapped with a multi-turn coil. Figure 1d and e shows the setup of the EPM cushion and suction slab. In addition to EPU, the shell of the EPM cushion in Fig. 1d is machined with silicon steel, providing sufficient strength and magnetic conductivity as the yoke. Moreover, the blank holder is embedded in silicon steel, as well as the void between the yoke and the EPU is filled with epoxy resin, which
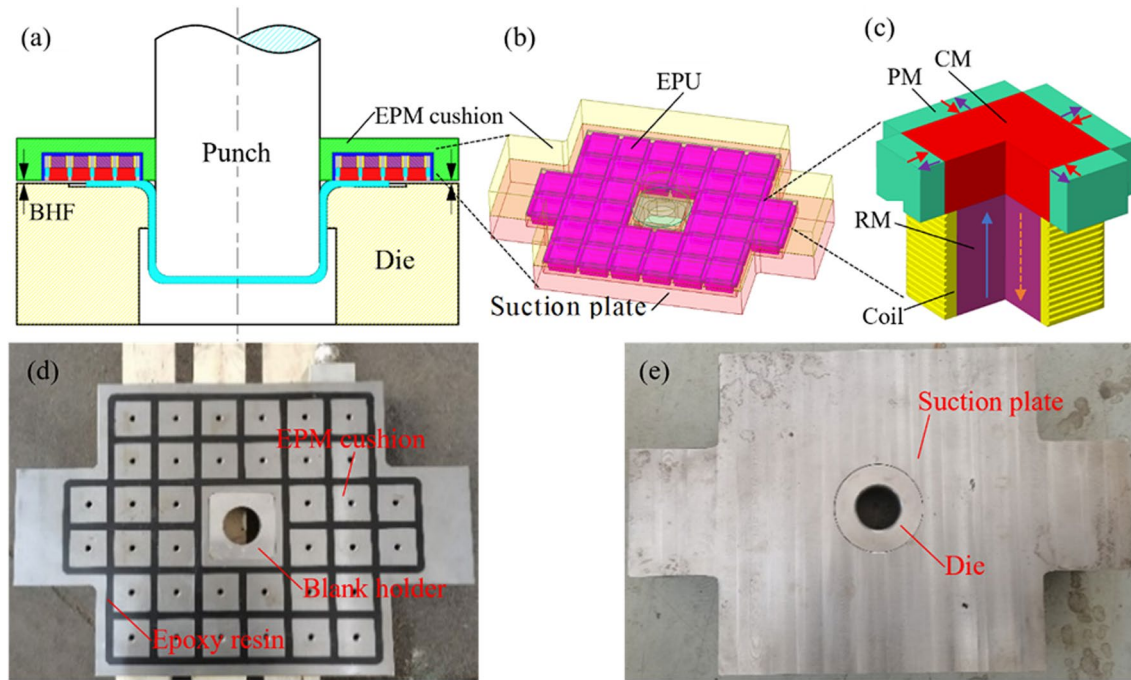
Fig. 1 Deep-drawing diagram (**a**), model (**b**) and detailed structure (**c**) as well as the device of EPM cushion (**d**) and suction plate (**e**)

Table 1 Magnetic parameters of material for EPM punching

Material	Coercivity (kA/m)	Relative permeability
Nd-Fe-B	890	1.05
Al-Ni-Co	90	3.5
Silicon steel	/	8500
Iron	/	4000
Epoxy/air	/	1

fixes spatial position and ensures adhesive strength. As seen in Fig. 1e, the groove of the suction plate inserted by concave mold is utilized to place the workpiece and keep almost constant clearance between the EPM cushion and the suction plate, which could improve the accuracy of controlling BHF amplitude and would be discussed detailly in Sect. 3.

The structure of the drawing device with EPM is introduced as above, and then the magnetic principle of loading and unloading BHF will be illustrated. Table 1 presents the magnetic properties of PM, RM, CM, yoke, and epoxy resin. It can be seen that the coercivity of PM is much greater than that of RM, whose magnetic field keeps almost constant when the external magnetic field changes within a certain range, while the magnetic field of RM could be changed in direction under the same condition, which provides the prerequisite of loading and unloading BHF.

As shown by the red arrow in Fig. 1c, the magnetization direction of PM is on the horizontal plane, pointing towards RM, while there is opposite magnetic field direction in adjacent EPU, namely, pointing outward RM (see the purple arrow in Fig. 1c). The magnetization direction of RM keeps in the vertical direction, which can be adjusted by reverse excitation current for its low coercivity. When the forward current is energized, the magnetization direction of RM is upward. According to the principle of the shortest magnetic circuit, the magnetic field would pass through the suction plate and return through adjacent magnets, as seen in the blue solid line arrow in Fig. 1c (see Fig. 2a). In addition, the BHF can be loaded and quantitatively analyzed by Maxwell's equation. During the drawing process, there is almost no displacement of the blank holder, so the binder force does almost no work, resulting in no need for continuous electrification to save energy. While when reverse current gets turned on, the magnetization direction of RM is downward. The magnetic field would return through PM and adjacent magnet without passing through suction plate, as seen in the orange dashed arrow in Fig. 1c (see Fig. 2b). As seen in the dashed arrow in Fig. 2b, the magnetic flux leakage loaded on the suction plate can be neglected in unloading states compared to loading state in Fig. 2a. So far, the principle of loading and unloading BHF has been explained qualitatively and then quantitative analysis will be performed in next section.
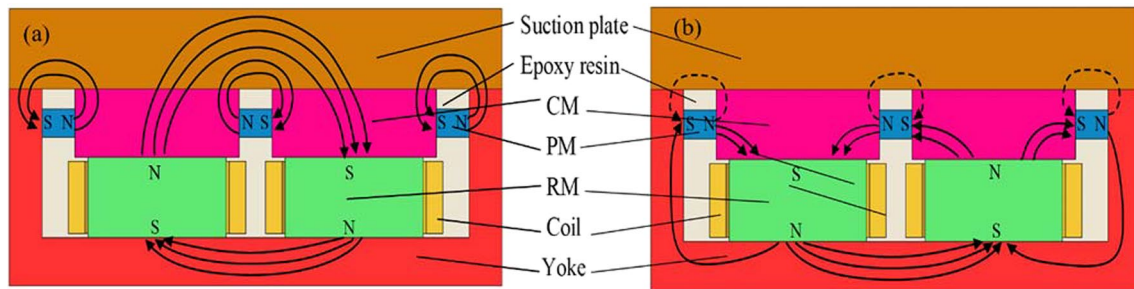
Fig. 2 The principle of magnetization. **a** Loading status. **b** Unloading status

3 Analysis of electromagnetic force

To investigate the deformation law of metal sheets including yield and plastic flow toward concave die, material behavior was modeled with Ludwik isotropic hardening model in deep drawing simulation with EPM blank holder, as seen in Eq. (1).

$$\sigma_{ys} = \sigma_{ys0} + k(\epsilon_{pe})^n \tag{1}$$

where σ_{ys}, σ_{ys0}, k, ϵ_{pe}, and n are the yield stress, initial yield stress, strength coefficient, plastic strain, and hardening index of metal material, respectively.

In the proposed deep drawing process with an EPM cushion, the magnitude of BHF is a crucial parameter, which is generated by magnetic attraction. The total attractive force exerted on the suction plate can be expressed as Eq. (2), which is the sum of the coupling effects of surface and internal magnetization currents.

$$F_B = \iiint_V I_V \times BdV + \iint_s I_S \times BdS \tag{2}$$

where F_B is the total electromagnetic attraction vector, namely, BHF, I_V, and I_S are the magnetization current intensity vector inside and on the surface of the sucked plate, respectively, V and S are the volume and surface area of the suction plate, respectively, and B is the magnetic induction intensity vector.

In the state of loading BHF, the superimposed magnetic field generated by the permanent magnet and reversible magnet will magnetize the suction plate. After being magnetized, magnetization currents would be generated inside and on the surface of the sucked plate, and the effect of the magnetic field on the molecular current is magnetic attraction. Besides, the internal and surface magnetization current density of the sucked plate can be expressed as Eqs. (3) and (4), respectively, while Eq. (5) represents the inherent magnetic properties of isotropic material.

$$I_V = L \times M \tag{3}$$

$$I_S = M \times n \tag{4}$$

$$M = \frac{\mu_r - 1}{\mu_r \mu_0} B \tag{5}$$

where M is the medium magnetization vector of the suction plate, n is the surface normal vector, μ_r is the relative permeability of the suction plate, μ_0 is the vacuum permeability, and L is the vector differential operator.

As seen in Fig. 1b, the sucked plate is a central symmetric structure, and the material of the sucked plate is assumed to be isotropic. Under these conditions, the magnetized current density on the surface of the sucked plate is still zero with the external magnetic field. Thus, Eq. (2) can be simplified as Eq. (6) and the scalar approximate solution can be further derived as Eq. (7):

$$F_B = \iiint_V I_V \times BdV = \frac{\mu_r - 1}{2\mu_r \mu_0} \iiint LB^2 dV \tag{6}$$

$$F_B = \frac{\mu_r - 1}{2\mu_r \mu_0} B_e^2 S \tag{7}$$

where B_e is the effective magnetic induction intensity at the interaction position between the magnetic field and the suction plate, and S is the interaction area between the electromagnetic cushion and the suction plate.

In the deep drawing process with EPMBH, the magnetic induction intensity is generated by the superposition of the excitation magnetic circuit and the permanent magnetic circuit, which can be quantitatively analyzed by Eq. (8).

$$B = B_r + B_P \tag{8}$$

where B_r and B_P are the magnetic induction intensity of the excited circuit and the permanent magnetic circuit, respectively.

The magnetic induction intensity of the permanent magnetic circuit is determined by the residual magnetism inside the permanent magnet, which can be described as

Eq. (9) with the structural parameters of the electromagnetic cushion.

$$B_P = \frac{B_1}{\pi}\left(\tan^{-1}\frac{AB}{2\delta_e\sqrt{A^2+B^2+4\delta_e^2}} - \tan^{-1}\frac{AB}{2(\delta_e+C)\sqrt{A^2+B^2+4(\delta_e+C)^2}} \right)$$
(9)

where A, B, and C are the length, width, and height of the permanent magnet, respectively, B_1 is the remanence of permanent magnet, and δ_e is the clearance between the suction plate and the electromagnetic cushion.

While the excitation magnetic field is generated by the coils energized with pulse currents. Moreover, the relationship between the magnetic field and current can be described by Maxwell's equation as below.

$$\nabla \times H = J \tag{10}$$

$$\nabla \cdot B_r = 0 \tag{11}$$

$$J = I_{coil}/A_c \tag{12}$$

where ∇ is the Hamilton operator, J is the vector of current density, I_{coil} is the current in the coil, and A_c is the cross-sectional area of the copper coil.

In theory, electromagnetic force comes from permanent magnets and excited coils, in which air permeability needs to be considered. In practical applications, the relative permeability of a conductive magnet is much greater than vacuum permeability, which can be ignored compared to the former, thus, BHF can be expressed as Eq. (13)

$$F_B = \frac{1}{2\mu}B^2 S = \frac{1}{2}BHS \tag{13}$$

According to Eq. (13), it can be concluded that the magnetic attraction acting on the sucked plate is mainly affected by the area of the interaction surface between the electromagnetic cushion and the sucked plate, as well as magnetic induction intensity is another determining factor. When the structural parameters of the electromagnetic cushion are

determined, it can be inferred from Eq. (9) that the magnetic induction intensity of a permanent magnetic circuit is a fixed value. Thus, the current intensity of the coil and the air gap between the suction plate and the electromagnetic cushion are the major influencing factors in the excited magnetic circuit, furthermore, the pulse current is controllable during magnetization and deep drawing process.

In simulation, COMSOL software was used to conduct finite element analysis on the electromagnetic cushion with 36 magnetic pole units, and the effect of loading condition on the electromagnetic force was analyzed. The pulse current in the electromagnetic cushion changed from 10 to 40 A, and the air gap ranged from 0 to 2 mm, respectively. The simulated magnetic flux density distribution on the work surface of the electromagnetic cushion is shown in Fig. 3a, and Fig. 3b presents the diagram of magnetic attraction with copper and steel plates relative to current and clearance, and it can be found that the magnetic attraction varies sharply with the increase of gap, while remains relatively stable with the change of current. Therefore, excitation current could be selected as the parameter for controlling magnetic force to improve accuracy and adjustability.

On the other hand, by comparing the magnetic attraction with copper and steel slabs under different currents, it can be concluded that the effect of the gap on the magnetic attraction caused by the magnetic properties of the plate first increases sharply and then slowly decreases. The two are almost equal without clearance (the difference is close to 0.15 kN). The difference between the two reaches the greatest value (the difference is close to 2.0 kN) with the clearance of 0.3 mm, due to the magnetic properties of the materials. As the gap continues to increase and the magnetic attraction decreases, the difference between the two gradually decreases (the difference is close to 1.0 kN with the clearance of 0.9 mm).

In the mold design of this paper, to ensure constant gap, there is a groove on the suction plate, whose depth is slightly less than the thickness of the thin sheet, as shown in Fig. 1e. When the suction plate interacts with the electromagnetic cushion through the metal plate, the gap between them is

Fig. 3 EPMBH. **a** Magnetic flux density distribution. **b** Electromagnetic attraction with copper and steel plates relative to mold clearance and excitation current
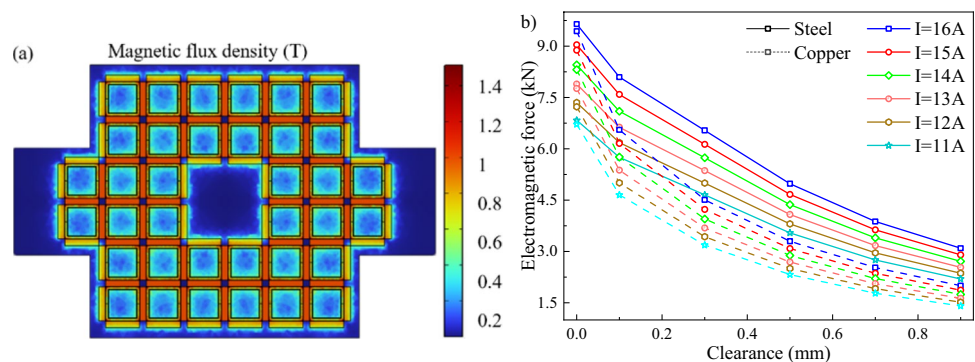
almost constant and close to zero. Therefore, due to the gap close to 0, the magnetic attraction of the copper plate is slightly smaller than that of the steel plate. It can be inferred that the magnetic properties of the material have a relatively small impact on the EPMBH device designed in this paper. Furthermore, with this method, the magnetic attraction could be precisely adjustable with different magnetization current intensities.

During the deep drawing process with an EPM electromagnetic cushion, the power-on time for each loading and unloading only needs to last for 20 ms for magnetization and demagnetization, respectively. The voltage of the power supply is 360 V, the unloading current remains constant at 20 A, and the loading current can be adjusted arbitrarily within the range of 0–40 A through the power controller to achieve variable BHF control. Thus, the energy consumption of the blank holder can be estimated by Eq. (14). After calculation, the energy required for each blank holder is 144–432 J, which is much lower than that of the hydraulic holding method.

$$W = UIt \qquad (14)$$

4 Experiment

4.1 Experimental device

Based on the above analysis, the controllability of BHF has been illustrated and the drawing mold was designed. Figure 4a presents the Y32-10T single-acting pressure machine and deep-drawing mold with EPM electromagnetic cushion utilized in the experiment. The suction plate is fixed on the base of the press machine, and the electromagnetic cushion is connected to the slider of the press through a sliding pull rod, which provides the prerequisite for the EPM electromagnetic cushion to remain stationary during the feed of the press. In the deep drawing process with EPMBH, the key parameters of average stamping speed and clearance are 0.5 m/s and 0.1 mm, respectively. The forming force and punch stroke were measured with pressure and displacement

sensors. Figure 4b shows the measuring equipment of VIALUX Autogrid comsmart, by which deep-drawing strain can be obtained and drawing performance can be evaluated accurately.

During the deep drawing process with EPM technology, the slide of the press goes down first. When the electromagnetic cushion comes into contact with the suction plate, the excitation current is applied to the coils, and the BHF is loaded. Next, the punch feeds to complete deep drawing and the demagnetization current is energized to unload BHF. In the end, the indenter exits and returns to its initial position, waiting for the next deep drawing. With this method for deep drawing, only two currents need to be applied at the magnetization and demagnetization moment of the electromagnetic cushion.

Figure 1a shows the 2D structure of deep drawing with EPM electromagnetic cushion, and all magnets are block structures. The diameter of coils is 1 mm and the number of turns is 200. Besides, the effective clearance of the electromagnetic cushion is 1 mm, which remains almost constant during the deep drawing process. Figure 5a and b present the punch and die used for the experiment, respectively, and the forming schematic diagram is shown in Fig. 5c. The material utilized in the experiment were 08-Al structural steel and H62 copper alloy with an initial diameter of 110 mm, whose property parameters are listed in Table 2. In addition, Tables 3 and 4 show the

Table 2 Property parameters of 08-Al structural steel and H62 copper alloy

Parameter	08-Al	H62
Density (g/cm^3)	7.8	8.43
Elastic modulus (GPa)	207	115
Yield strength (MPa)	185	120
Tensile strength (MPa)	325	385
Poisson's ratio	0.3	0.34
Elongation rate (%)	28	15
Thickness (mm)	0.8	

Fig. 4 Experimental apparatus. **a** Single-acting pressure machine, mold, and sensing equipment. **b** Strain scanner and drawn specimens
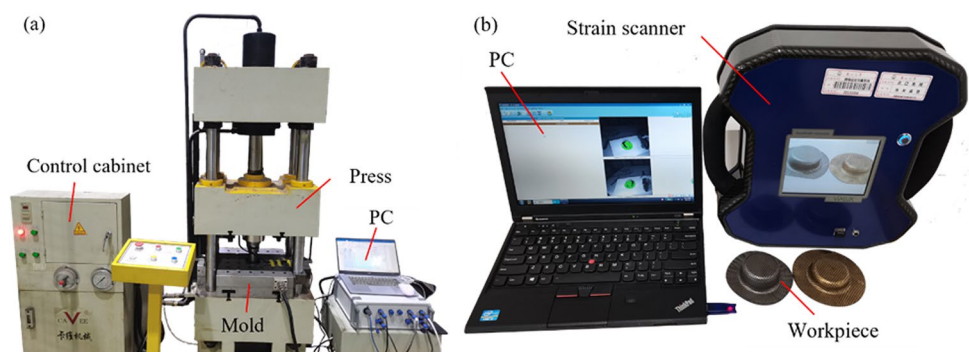
Table 3 Chemical composition of 08-Al

Component	C	Fe	Si	Mn	Cr	Ni	P	S	Cu	Al
Mass fraction (ωt.%)	0.1	99	0.03	0.45	0.1	0.3	0.03	0.03	0.25	0.02~0.07

Table 4 Chemical composition of H62

Component	Cu	Fe	Pb	Sb	Bi	P	Impurity	Zn
Mass fraction (ωt.%)	60.5~63.5	0.15	0.08	0.005	0.002	0.01	0.5	Rest

Fig. 5 Structure of deep drawing with EPM. **a** Punch. **b** Die. **c** Schematic diagram
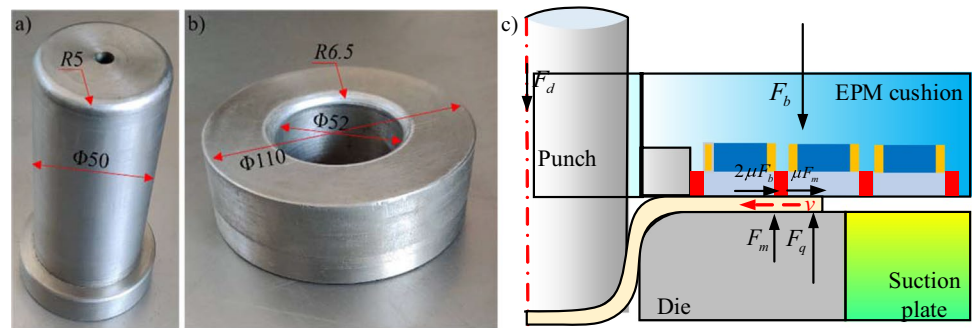
Table 5 Simulated BHF with copper and steel plates under different currents

Current (A)	11	12	13	14	15	16
Copper	6.72	7.23	7.76	8.31	8.88	9.44
Steel	6.84	7.35	7.89	8.46	9.04	9.65

Table 6 The forming height under the selected currents

Current (A)	Copper		Current (A)	Steel	
	Height (error)	State		Height (error)	State
11	15.3 (0.62)	Wrinkling	12	17.5 (0.45)	Wrinkling
13	19.7 (0.25)	Safe	14	22.4 (0.19)	Safe
15	18.6 (0.42)	Crack	16	20.8 (0.38)	Crack

Fig. 6 Drawing simulation results with EPM technology: non-ferromagnetic copper plate with the current of 11 A (**a**), 13 A (**b**), and 15 A (**c**); ferromagnetic steel sheet with the current of 12 A (**d**), 14 A (**e**), and 16 A (**f**)
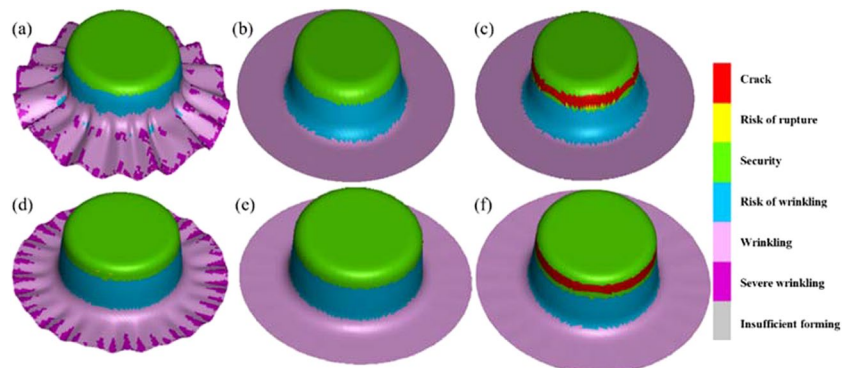
chemical composition of 08-Al and H62, respectively. In subsequent analysis, the path starts from the center of the sheet to the edge, and its dimension is the distance from the analysis position to the symmetrical centerline. In the experiment, three samples were tested for each condition, and reducing friction was realized by lubricating the surface of the metal slab. The friction coefficient was set to 0.125 in the simulation.

4.2 Forming performance analysis

Figures 6 and 7 show the deep drawing results based on simulation and experiment, respectively, and there is good consistency. As shown in Fig. 6a and d, an EPM electromagnetic cushion with a small excitation current could not provide sufficient BHF, resulting in the problem of wrinkling. While excessive current would suppress metal flow, rupture may occur, as seen in Fig. 6c and f. Therefore, there is an optimal current value for deep drawing height without defects, as shown in Fig. 6b and e. Detailly, Table 5 shows the simulated BHF with copper and steel plates under different currents. According to the drawing results in Fig. 7, the optimal current

value of ferromagnetic steel is greater than that of non-ferromagnetic copper, where there could be a complex effect of magnetism and stiffness simultaneously. Moreover, the forming height and state are listed in Table 6 under the three selected current conditions, in which the height and error are the average height and its standard deviation, respectively.

Figure 8 shows the measured forming force curve at different currents for the 08-Al steel and H62 copper plate. As shown in Fig. 8a, there is a reduction in the forming force after local rupture and wrinkling for the steel plate because of the reduction of the forming cross-sectional area and average strain, while the phenomenon is more significant for copper slabs due to more severe wrinkling. After complete

Fig. 7 Drawing experiment results with EPMBH: non-ferromagnetic copper plate with the current of 11 A (**a**), 13 A (**b**), and 15 A (**c**); ferromagnetic steel sheet with the current of 12 A (**d**), 14 A (**e**), and 16 (**f**)
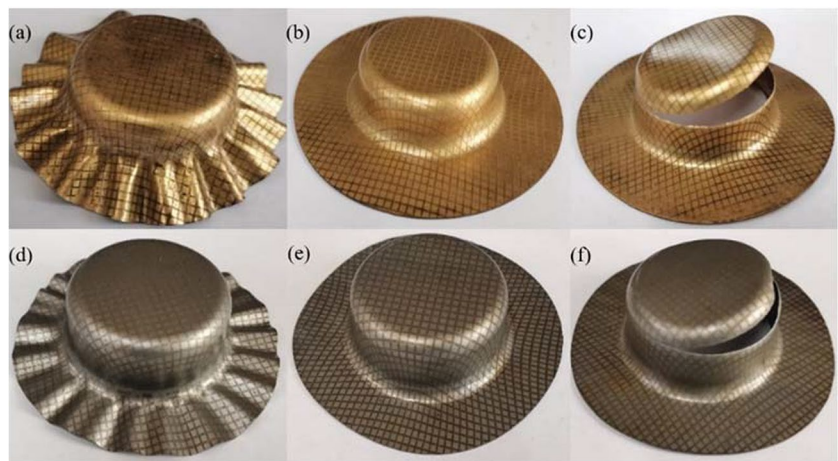

Fig. 8 Forming force versus displacement curve at different currents. **a** Steel sheet. **b** Copper plate
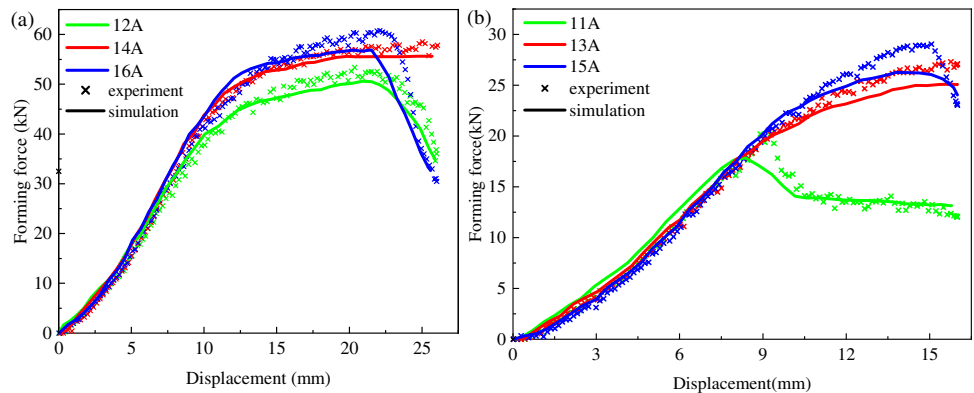

Fig. 9 Measured result of thinning of drawn workpiece. **a** Copper plate. **b** Steel plate
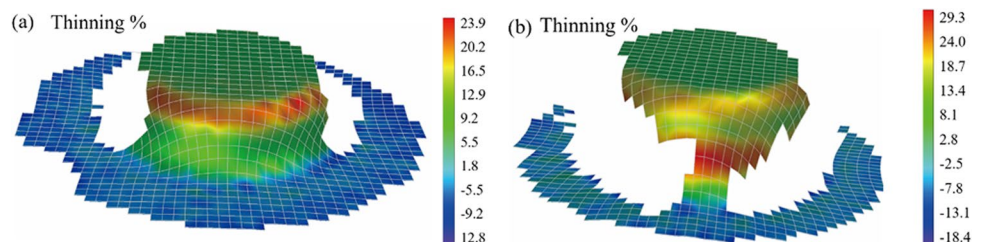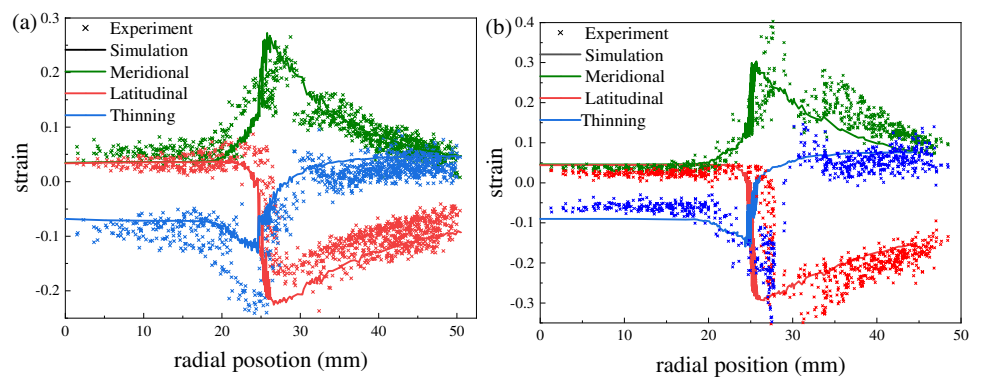
Fig. 10 Strain measured result in simulation and experiment. **a** Copper plate. **b** Steel plate

5 Conclusion

The common blank holder methods, such as hydraulics, rubber, and spring, can only perform a single loading path for BHF, whose mechanisms are complex and costly. The combination of EPM technology and blank holder technology can alleviate this problem effectively. In the paper, the forming performance with EPM blank holder technology was investigated in detail, and the main conclusion can be drawn as follows:

(1) Compared with conventional blank holder methods, the BHF can be controllable arbitrarily with the EPM blank holder technique, through adjusting the amplitude of the excitation current. Moreover, the proposed blank holder method can simply the structure of the forming equipment, conducive to lightweight design.

(2) The magnetic attraction generated by the electromagnetic cushion can fully meet the requirements of the blank holding function. In the experiment, the optimal excitation current was 14 A for the steel plate, while it was 13 A for the copper sheet.

(3) Ferromagnetic and non-ferromagnetic materials were utilized to perform forming tests, the result shows that with metal plates, the magnetic properties of the materials play little effect on BHF and drawing performance. The reason could be that BHF is mainly from the interaction between the electromagnetic cushion and the suction slab, while the thin plate to be formed is not in the critical magnetic field zone and whose impact on the overall magnetic field could be negligible.

(4) With the EPMBH method, the energy consumption is only 144–432 J, while it would be continuously consumed with other blank holder methods, such as hydraulics and gas cushion. Furthermore, through maintaining a constant gap, the precise control problem of BHF was analyzed theoretically and confirmed experimentally.

wrinkling, the copper sheet enters the deep drawing stage again, as shown in Fig. 8b, which can also be confirmed from the secondary drawing traces in Fig. 7a.

Figure 9 shows the thinning measured results of the drawn workpiece with copper and steel plates, and the results show that there is no significant deformation at the bottom of the cylindrical part while thickening occurs in the flange area. Furthermore, the thinning phenomenon is obvious in the sidewall and rounded area. Comparing Fig. 9a with b, the forming height for the steel sheet is higher than that of the copper sheet would cause a greater thinning and thickening rate. For the copper plate, there was a maximum strain and fracture danger zone at the punch fillet, while these occurred at the side wall of the steel slab in the experiment. The possible reason is the good toughness for copper alloy, which is a poor performance for steel plate accompanied by bending and reverse bending processes during the deep drawing.

Figure 10 presents the strain of copper and steel plates without defects at excitation currents of 13 A and 14 A, respectively. It can be seen that the experimental results are consistent with the simulation results, and the bottom area of the cylindrical part is close to biaxial stretching. Thus, meridional and latitudinal strains were almost equal and constant. The deformation was mainly concentrated in the side wall and fillet area, as well as its peak value is determined by the depth of the drawing. The metal in the flange area flows towards the concave mold for replenishment, resulting in sheet thickness gradually increasing along the radial direction and the BHF mainly acts on the flange edge ultimately. Furthermore, the phenomenon aggravates the uneven distribution of plate thickness, causing little strain in the flange edge area in Fig. 10a and b. Compared with Fig. 10a, there was a deviation between simulation and experiment in Fig. 10b, whose main reason is excessive deformation led to strain divergence in deformation zone before rupture. In the region of the side wall and concave mold fillet, strain data points were difficult to fully measure due to large deformation and complex spatial structure.

Declarations

Conflict of interest The authors declare no competing interests.

References

1. Shi YQ (2010) Improving the quality in deep drawing of rectangle parts using variable blank holder force. Appl Mech Mater 37:521–524

2. Hassan MA, Suenaga R, Takakura N, Yamaguchi K (2005) A novel process on friction aided Deep drawing using tapered blank holder divided into four segments. J Mater Process Technol 159(3):418–425

3. Lee JS, Hong SJ, Yu WR, Kang TJ (2007) The effect of Blank Holder Force on the Stamp forming behavior of Non-crimp Fabric with a chain stitch. Compos Sci Technol 67(3–4):357–366

4. Ayachi N, Guermazi N, Manach P (2021) Effect of blank-holder force on springback of ultra-thin copper sheets. Materials Science and Engineering, IOP Publishing

5. Sheng ZQ, Jirathearanant S, Altan T (2004) Adaptive Fem Simulation for Prediction of Variable Blank Holder Force in Conical Cup drawing. Int J Mach Tools Manuf 44(5):487–494

6. Kitayama S, Shimizu K, Kawamoto K (2021) Numerical Optimization of Blank Shape and sloped variable blank holder force trajectory for an Automotive Part. J Adv Mech Des Syst Manuf 15(3):2389–2400

7. Wang HT, Kong JF, Pan HB, Fang JX, Shen XH (2022) Influence of the key process parameters in Hydrodynamic Deep drawing utilizing a combined floating and static die cavity. Int J Adv Manuf Technol 120(9–10):5673–5685

8. Tran MT, Shan ZT, Lee HW, Kim DK (2021) Earing reduction by Varying Blank Holding Force in Deep drawing with deep neural network. Metals 11(3):395

9. Li LC, Li MZ, Wang XW (2013) The technology of flexible blank holder forming and the study of its numerical simulation. Appl Mech Mater 490:776–780

10. Chen MH, Wang FD, Xiong J (2012) Numerical simulation of rubber bladder hydroforming process for shrink flanging parts with large curvature. Int Conf Front Adv Mater Eng Technol 1286–1289

11. Sun G, Li MZ, Yan XP, Zhong PP (2007) Study of blank-holder technology on Multi-point forming of thin sheet metal. J Mater Process Technol 187:517–520

12. Wang ZJ, Zheng LH, Liu ZG, Xiang N, Wang PY (2016) Investigation of Viscous pressure forming for 6k21-T4 aluminum Alloy Car panels. Int J Adv Manuf Technol 85(9–12):2525–2534

13. Luyen TT, Banh TL, Tran TV, Nguyen DT (2019) A study on a deep-drawing process with two shaping States for a fuel-Filter Cup using combined Simulation and Experiment. Adv Mech Eng 11(8):1062–1067

14. Li H, Wang Q, He F (2018) Design and Fe simulation of a novel electromagnetic blank holder system in sheet metal drawing process. Chinese Control And Decision Conference (CCDC), IEEE

15. Huang YJ, Han XT, Cao QL, Lai ZP, Cai H, Liu N, Li XX, Chen M, Li L (2010) Design and analysis of a pulsed electromagnetic blankholder system for electromagnetic forming. Procedia Eng 207:347–352

16. Zhang HS, Qin SJ (2022) A novel process of Deep drawing based on Electro-Permanent Magnet combined segmental blank holder technique. Int J Adv Manuf Technol 118(11–12):3883–3896

17. Qin SJ, Zhang HS, Mao YB, Yang L, Li XB, Hu ZH, Cheng X (2020) Electropermanent Magnet Blank Holder Technique in sheet metal Deep drawing. Int J Adv Manuf Technol 106(11–12):5497–5507

18. Qin SJ, Cheng X, Zhang HS, Lu TJ, Gu TT, Meng LY (2020) Analyses of Thermal Field and coupled magnetic-mechanical field in Electro-Permanent Magnet blank holder technique. Int J Adv Manuf Technol 110(1–2):499–510

19. Zhang HS, Qin SJ, Cao LQ, Meng LY, Zhang QR, Li C (2020) Research on Deep drawing process using radial segmental blank holder based on Electro-Permanent Magnet Technology. J Manuf Process 59:636–648